

AD-A134 502

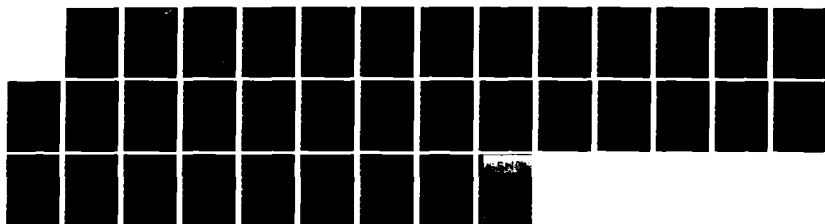
FORMATION AND PROPERTIES OF POLYMERS USED IN ORGANIC
MATRIX COMPOSITES(U) PRINCETON UNIV NJ J K GILLHAM
SEP 83 ARD-16822 4-MS DRAG29-80-K-0041

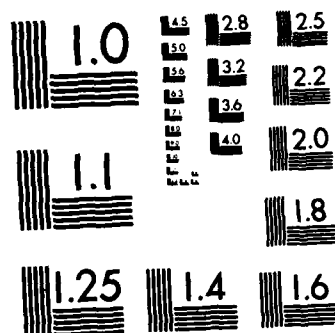
1/1

UNCLASSIFIED

F/G 11/9

NL





MICROCOPY RESOLUTION TEST CHART
NATIONAL BUREAU OF STANDARDS-1963-A

12

A134502

DTIC FILE COPY

EDITION OF 1 NOV 65 IS OBSOLETE

SECURITY CLASSIFICATION OF THIS PAGE (When Data Entered)

83 11 07 022

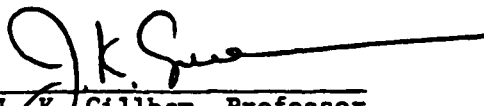
Accession For	
NTIS GRA&I	<input checked="" type="checkbox"/>
DTIC TAB	<input type="checkbox"/>
Unannounced	<input type="checkbox"/>
Justification	
By	
Distribution/	
Availability Codes	
Dist	Avail and/or Special
A/1	



PRINCETON UNIVERSITY
Department of Chemical Engineering
Polymer Materials Program
Princeton, New Jersey 08544

FINAL REPORT TO THE
U.S. ARMY RESEARCH OFFICE
RESEARCH TRIANGLE PARK, NC 27709
for
ARMY RESEARCH OFFICE CONTRACT NUMBER DAAG29-80-K-0041

TITLE: FORMATION AND PROPERTIES OF POLYMERS USED
IN ORGANIC MATRIX COMPOSITES


J. K. Gilham, Professor
Principal Investigator
Telephone: 609/452-4694

SEPTEMBER 1983

DTIC
ELECTE
S NOV 8 1983 D

DISTRIBUTION STATEMENT A
Approved for public release;
Distribution Unlimited

FORMATION AND PROPERTIES OF THERMOSETTING MATERIALS: STATEMENT OF PROBLEM

Composite materials involving an organic matrix reinforced with continuous filaments having a high tensile modulus and strength are important in applications requiring light-but-strong structures. In such materials the organic matrix is generally formed by the chemical conversion of a reactive fluid to a solid in the thermosetting process. Although thermoplastic materials can also be used, they are of limited application because of the high viscosity of their melts, their relative dimensional instability under load, and their unsuitable composite performance above the load-limiting transitions of the organic matrix (i.e. the glass transition temperature, T_g , for amorphous and the melting temperature, T_m , for semicrystalline polymers).

The most important thermosetting matrices involve network systems such as the epoxies, and semi-ladder polymers such as the polyimides. The proper exploitation of these materials is currently restricted because of the unsatisfactory state of the scientific and technical information available concerning the interdependence of their chemistry and their mechanical properties. Fundamental reasons for this include a lack of understanding of the cure process and of the nature of the glassy state. However, from the experimental point of view, they are also inherently difficult materials to study. They are infusible and insoluble and are therefore synthesized and fabricated in one operation: because of this, their chemistry and physics are strongly coupled. The amorphous nature of the materials also restricts the applicability of diffraction and morphological techniques that can be used with crystalline and oriented samples.

The very intractability which makes the characterization of thermosetting materials difficult is associated with the reasons for their superior engineering behavior. A material property of particular importance that is related to the nature of the molecular networks is their dimensional stability under mechanical stress. However, in the unreinforced state the materials are often brittle and they must therefore then be used in structural applications in the form of fiber-reinforced composites or chemically produced two-phase rubber-modified materials. The current interest in composites makes it essential to understand the physical properties of these organic matrices in relation to their chemistry. Again, from the practical point of view, it is to be noted that homogeneous unreinforced specimens are often difficult to prepare in a defect-free state for testing because of residual curing and thermal shrinkage stresses, bubble inclusions introduced during cure, and surface defects introduced during test specimen preparation. In addition, the chemical approach to the study of molecular structure-bulk property relations has been made difficult because of the ubiquitous use of impure reactants, proprietary formulations, and arbitrary curing conditions. Each of these factors becomes of greater importance as the performance expected from the composite is increased.

Even with pure reactants the complexity and competing nature of the chemical reactions involved in synthesizing the network materials would make molecular structure-bulk property correlations difficult to obtain. What is required is a more general understanding of the key relationships between the process of cure and the properties of the cured state. It is to this point that the research has been directed.

FORMATION AND PROPERTIES OF THERMOSETTING MATERIALS: A SUMMARY

Abstract

A generalized time-temperature-transformation (TTT) cure diagram for thermosetting systems is discussed from the point of view of understanding the cure behavior, properties, and degradation of thermosetting systems.

Introduction

Research in this laboratory has shown that a time-temperature-transformation diagram (analogous to the TTT diagrams that have been employed for many years in metallurgical processing) may be used to provide an intellectual framework for understanding and comparing the cure and physical properties of thermosetting systems (1-5). Isothermal TTT diagrams such as that shown in Figure 1 can be obtained by measuring the times to events which occur during isothermal cure versus temperature (T_{cure}). The events include phase-separation (for example, in rubber-modified systems -- not shown in Figure 1), gelation, vitrification, and devitrification. Gelation is synonymous with the incipient formation of an infinite network. Vitrification occurs when the glass transition rises through the isothermal temperature of cure. Devitrification occurs when the glass transition temperature decreases through the isothermal temperature. The diagram displays the distinct states encountered due to chemical reactions. These states include liquid, gelled rubber, ungelled glass, gelled glass, and char. The diagram also displays the critical temperature $T_{g\infty}$, $_{\text{gel}}T_g$, and T_{g0} which are, respectively, the glass transition temperature of the fully cured system, the temperature at which the times to gelation and to vitrification are the same, and the glass transition temperature of the unreacted reactants.

The TTT diagram shown in Figure 1 can be obtained conveniently using a technique (TBA) in which a resin-impregnated glass braid is the specimen in a torsion pendulum (1, 6). Use of the composite specimen permits monitoring of the changes from liquid to rubber to glass, and to devitrification, which can occur on cure. Relationships between cure and properties (e.g., transitions) can be obtained from temperature scans of the cured specimens.

Discussion

Much of the behavior of thermosetting materials can be understood immediately in terms of the TTT diagram (Figure 1) through the influence of the gelation, vitrification, and devitrification events on properties: gelation limits macroscopic flow, and limits growth of a dispersed phase (as in rubber-modified systems); vitrification limits chemical conversion; devitrification marks the limit in time due to degradation for the material to support a load. Thus (in listed form):

- a) The ungelled glassy state is the basis of commercial molding and "prepreg" materials since, on heating, the ungelled material will flow before gelling.
- b) Temperature $_{\text{gel}}T_g$ is a critical temperature in determining the upper temperature for storing reactive materials to avoid gelation.
- c) The morphology developed in a two-phase system (e.g., those in which rubber-rich domains precipitate as a dispersed phase) on isothermal cure depends on the gelation temperature. The reaction temperature determines the competition between thermodynamics and kinetic (transport) factors. For optimum mechanical properties, a two-phase system will be cured at one temperature to control the morphology, and subsequently cured above $T_{g\infty}$ to complete the reactions of the matrix.

- d) Shrinkage stresses due to cure begin to develop at gelation. There is a need to develop polymerization systems involving low shrinkage on cure.
- e) Isothermal cure at temperature T_{cure} below $T_{g\infty}$ will (in principle) lead to $T_g = T_{\text{cure}}$. There is a need to develop mechanisms of cure which yield $T_g \gg T_{\text{cure}}$.
- f) Complete cure is obtained (in principle) only by curing above $T_{g\infty}$. Correlations between macroscopic behavior and molecular structure will then result only after curing above $T_{g\infty}$.
- g) For high $T_{g\infty}$ systems there is a competition between cure and degradation.
- h) The limiting viscosity in the fluid state is controlled by gelation above temperature $_{\text{gel}}T_g$, and by vitrification below temperature $_{\text{gel}}T_g$. At gelation the weight average molecular weight and zero shear rate viscosity become infinite. Viscosity in the vicinity of vitrification is described by the Williams-Landel-Ferry equation.
- i) Isothermal reactions proceed slowly after vitrification. Below temperature $_{\text{gel}}T_g$ this leads eventually to gelation. At high temperatures this leads eventually to degradation. Degradation can result in devitrification as the glass transition temperature decreases through the isothermal temperature due to decrease in crosslinking, or formation of low molecular weight plasticizing material. Degradation can also result in vitrification (e.g., char formation) as the glass transition rises through the isothermal temperature due to increase in crosslinking or volatilization of low molecular weight plasticizing material.
- j) The times to gelation and to vitrification each can be computed from the reaction mechanism (or the reaction rate dependence on the concentrations of the reactants) and the extent of reaction at gelation (which is constant according to Flory's theory of gelation) and the extent of reaction at vitrification, respectively. Since vitrification occurs when the glass transition temperature rises to the temperature of cure, computation of the time to vitrify involves knowledge of the relationship between T_g and conversion.

The following is an outline for computation of the times to gelation and to vitrification. The overall reaction rate is a function of the temperature (T), extent of reaction (X), reaction mechanism $f(X)$, and local microviscosity (η_L) which in turn is a function of the molecular weight and temperature.

$$\frac{dX}{dt} = A \exp(-E_A/RT) f(X) f(\eta_L) \quad (\text{I})$$

Analysis of an epoxy system showed that diffusion influenced the reaction rate only at vitrification (4). The general kinetic equation describing the reaction is then

$$\frac{dX}{dt} = A \exp(-E_A/RT) f(X). \quad (\text{II})$$

The time to reach gelation

$$t_{\text{gel}}^* = \exp(Ar/T^*) \int_0^{X_{\text{gel}}} \frac{dX}{f(X)} \quad (\text{III})$$

and the time to reach vitrification

$$t_{\text{vit}}^* = \exp(Ar/T^*) \int_0^{X_g(T^*)} \frac{dX}{f(X)} \quad (\text{IV})$$

where $t_{gel}^* = At_{gel}$ and $t_{vit}^* = At_{vit}$ are the dimensionless times to reach gelation and vitrification, respectively; $T^* = T/Tg_0$ is a dimensionless temperature, and $Ar = E_A/RTg_0$ is the Arrhenius number. X_{gel} and X_g are the extent of conversion of reactants at gelation and vitrification, respectively. The times to gelation and to vitrification can be computed using these equations (III and IV), knowledge of X_{gel} (for gelation) and a relationship between X_g and Tg (for vitrification), and the reaction kinetics (7).

The "S"-shaped vitrification curve obtained experimentally has been matched theoretically for one epoxy system from temperature Tg_0 to temperature Tg_∞ (4).

k) The vitrification curve is "S"-shaped for both network- and linear-forming step-growth reactions (8). At temperatures immediately above Tg_0 the time to vitrification passes through a maximum in consequence of the opposing influences of the temperature dependence of the viscosity and reaction rate constant. At higher temperatures the time to vitrification passes through a minimum in consequence of the opposing influences of the reaction rate constant and the decreasing concentration of reactive sites at vitrification as Tg_∞ is approached.

l) The fractional extent of reaction at vitrification and the time to vitrify, like gelation, decrease with increasing functionality (5).

m) For epoxies the reactions become diffusion controlled in the vicinity of vitrification (4).

n) The reaction mechanism of a particular thermosetting system in principle can be deduced from the shape of the experimentally measured "S"-shaped vitrification curve.

o) Increasing cure time leads at the curing temperature to increasing conversion, Tg , crosslinking density, and density. Prior to vitrification the modulus at the curing temperature also increases. However in the glassy state at room temperature, the corresponding modulus and density can decrease whereas absorption of water can increase with increasing extent of cure (9). This apparently anomalous behavior is probably a consequence of the non-equilibrium nature of the glassy state: it follows that the higher the glass transition temperature the further the room temperature properties are from equilibrium (10).

References

1. J. K. Gillham, "Torsional Braid Analysis (TBA) of Polymers", in Developments in Polymer Characterisation-3. J. V. Dawkins, Ed., Applied Science Publishers, London, 1982, Ch. 5, pp. 159-227.
2. J. K. Gillham, "The Time-Temperature-Transformation (TTT) State Diagram and Cure", in The Role of the Polymer Matrix in the Processing and Structural Properties of Composite Materials. J. C. Seferis and L. Nicolais, Ed., Plenum Press, New York, 1983, pp. 127-145.
3. J. B. Enns and J. K. Gillham, "Torsional Braid Analysis: Time-Temperature-Transformation Cure Diagrams of Thermosetting Epoxy/Amine Systems", in Polymer Characterization: Spectroscopic, Chromatographic, and Physical Instrumental Methods. C. D. Craver, Ed., American Chemical Society, Advances in Chemistry Series, No. 203, pp. 27-63, 1983.
4. J. B. Enns and J. K. Gillham, "The Time-Temperature-Transformation (TTT) Cure Diagram: Modeling the Cure Behavior of Thermosets, Journal of Applied Polymer Science, Vol. 28, pp. 2567-2591 (1983).
5. H. N. Naé and J. K. Gillham, "Time-Temperature-Transformation (TTT) Diagrams of High Tg Epoxy Resins: Competition Between Cure and Degradation", American Chemical Society, Preprints, Division of Organic Coatings and Plastics Chemistry, Vol. 48, pp. 566-570, 1983.

6. J. B. Enns and J. K. Gillham, "Automated Torsion Pendulum: Control and Data Collection/Reduction Using a Desktop Computer", in Computer Applications in Applied Polymer Science, T. Provder, Ed., American Chemical Society Symposium Series, No. 197, pp. 329-352, 1982.
7. H. E. Adabbo and R. J. J. Williams, "The Evolution of Thermosetting Polymers in a Conversion-Temperature Phase Diagram", J. Applied Polymer Science, Vol. 27, 1327-1334 (1982).
8. M. T. Aronhime and J. K. Gillham, "The Transformation of Liquid to Amorphous Solid: Effect of Reaction Mechanism on the Time to Vitrify for Linear and Network Polymerization", Journal of Coatings Technology, submitted May, 1983.
9. J. P. Aherne, J. B. Enns, M. J. Doyle, and J. K. Gillham, "Modulus, Density and Water Absorption in Glassy Polymers Versus Extent of Cure", American Chemical Society. Preprints, Division of Organic Coatings and Plastics Chemistry, Vol. 46, pp. 574-579, 1982. Also: Journal of Applied Polymer Science. Production Number 1302W, September 1983.
10. A Shimazaki, Journal of Polymer Science, Pt. C., Vol. 23, 555 (1968).

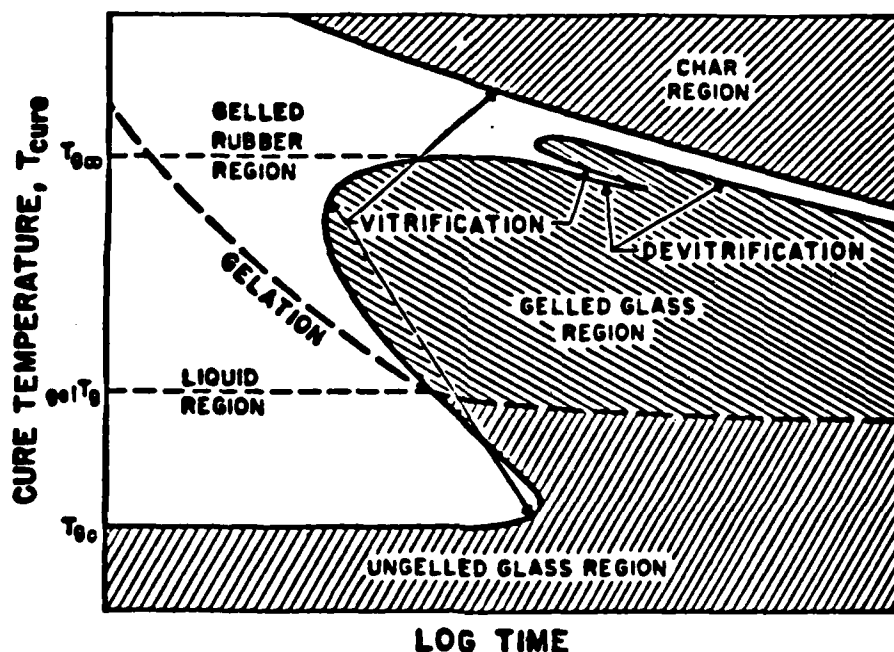


Figure 1

Time-Temperature-Transformation (TTT) Cure Diagram of a Thermosetting Polymer, showing three critical temperatures ($T_{g\infty}$, $gelT_g$, T_{g0}) and four distinct states of matter (liquid, gelled rubber, gelled glass, ungelled glass). Vitrification can occur in some systems above $T_{g\infty}$ in consequence of degradation (5).

FORMATION AND PROPERTIES OF THERMOSETTING MATERIALS: PUBLICATION

John B. Enns and John K. Gillham, "Time-Temperature-Transformation (TTT) Cure Diagram: Modeling the Cure Behavior of Thermosets", Journal of Applied Polymer Science, Vol. 28, pp. 2567-2591 (1983).

Time-Temperature-Transformation (TTT) Cure Diagram: Modeling the Cure Behavior of Thermosets

JOHN B. ENNS* and JOHN K. GILLHAM, *Polymer Materials Program, Department of Chemical Engineering, Princeton University, Princeton, New Jersey 08544*

Synopsis

The times to gelation and to vitrification for the isothermal cure of an amine-cured epoxy (Epon 828/PACM-20) have been measured on macroscopic and molecular levels by dynamic mechanical spectrometry (torsional braid analysis and Rheometrics dynamic spectrometer), infrared spectroscopy, and gel fraction experiments. The relationships between the extents of conversion at gelation and at vitrification and the isothermal cure temperature form the basis of a theoretical model of the time-temperature-transformation (TTT) cure diagram, in which the times to gelation and to vitrification during isothermal cure versus temperature are predicted. The model demonstrates that the "S"-shape of the vitrification curve depends on the reaction kinetics, as well as on the physical parameters of the system, i.e., the glass transition temperatures of the uncured resin (T_{g0}), the fully cured resin ($T_{g\infty}$), and the gel ($T_{g\text{gel}}$). The bulk viscosity of a reactive system prior to gelation and/or vitrification is also described.

INTRODUCTION

The isothermal cure of thermosetting resins is usually characterized by gelation and vitrification: gelation corresponds to the incipient formation of an infinite network of crosslinked polymer molecules, and vitrification involves a transformation from a liquid or rubbery state to a glassy state as a result of an increase in molecular weight. The cure of thermosetting resins is complicated by the interaction of the chemical kinetics and the changing physical properties. Near vitrification, the kinetics are affected by the local viscosity, which in turn is a function of the extent of reaction and temperature. Thus the cessation of reaction is not necessarily an indication that the reaction is complete, i.e., the reaction may have been quenched due to vitrification. Subsequent exposure to temperatures greater than the temperature of cure could result in further reaction.

The concept of a state diagram has been developed¹ in an attempt to understand cure phenomena. A time-temperature-transformation (TTT) cure diagram (Fig. 1) is a plot of the times required to reach gelation and vitrification, respectively, during isothermal cure as a function of cure temperature. Gelation, which occurs at a fixed extent of conversion^{2,3} as long as the reaction mechanism is not a function of temperature, is responsible for the transformation from a liquid to a rubbery state,^{2,4} since the network has elastic properties not present in the low molecular weight linear or branched resin. Vitrification occurs when the glass transition increases to the temperature of cure and marks the transformation from a rubber to a gelled glass (if gelation has occurred) or from a liquid

* Present address: Bell Telephone Laboratories, Whippany, N.J. 07981.

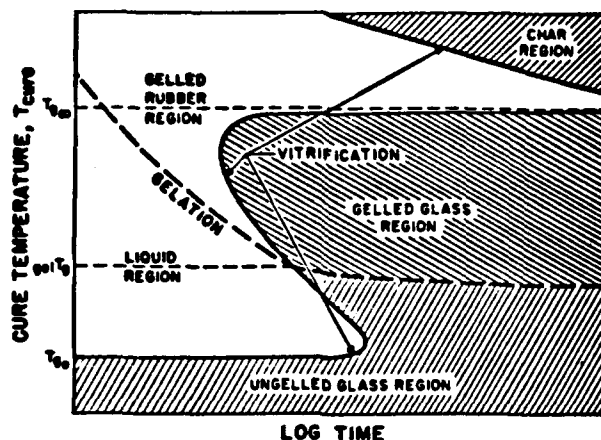


Fig. 1. Generalized time-temperature-transformation (TTT) cure diagram. A plot of the times to gelation and vitrification during isothermal cure vs. temperature delineates the regions of four distinct states of matter: liquid, gelled rubber, gelled glass, and ungelled glass. (Vitrification can occur in some systems above $T_{g\infty}$ in consequence of degradation.)

to an ungelled glass (if gelation has not occurred). Below $_{gel}T_g$, the temperature at which the time to gel is the same as the time to vitrify, the resin can remain ungelled, even though it becomes hardened during storage. The resin remains processable and fusible as long as it is in its ungelled state. Below T_{g0} , the glass transition temperature of the freshly mixed uncured resin, essentially no reaction occurs because the reactive species are immobilized in the glassy state.

The resin will not vitrify on isothermal cure if the cure temperature is above $T_{g\infty}$, the glass transition temperature of the fully cured resin. The cure can then proceed to completion since it will not be quenched prematurely as it would be below $T_{g\infty}$, although 100% conversion is rarely achieved because some reactive sites may be isolated in the network. Other competing reactions such as degradation can occur; the temperatures at which they occur can overlap with $T_{g\infty}$, resulting in a situation where the resin may never be fully cured because of these conflicting processes.⁵

The vitrification curve is "S"-shaped (Fig. 1). At temperatures immediately above T_{g0} the time to vitrification passes through a maximum in consequence of the opposing influences of the temperature dependence of the viscosity and the reaction rate constant. At higher temperatures the time to vitrification passes through a minimum in consequence of the opposing influences of the reaction rate constant and the decreasing concentration of reactants at vitrification as $T_{g\infty}$ is approached.

To characterize the curing phenomena of thermosetting resins, several complementary techniques can be utilized to obtain information on a macroscopic as well as a molecular level. Dynamic mechanical experiments permit the cure process to be monitored on a macroscopic level by measuring the elastic and loss moduli as the resin changes from liquid to rubber and eventually to glass. Isothermal experiments provide times to gelation and vitrification, and subsequent temperature scans provide thermomechanical spectra which characterize the state of cure of the resin. The entire cure process from liquid to solid can be monitored using the torsional braid analysis (TBA) technique because it utilizes a supported specimen; the Rheometrics Dynamic Spectrometer (RDS) used in

the dynamic oscillatory shear mode (parallel plates) is limited to the time to vitrification. On a molecular level, the infrared spectrum of an epoxy resin exhibits three absorption bands characteristic of the epoxide group: 1250 cm^{-1} ; between 950 and 860 cm^{-1} (typically 915 cm^{-1}); and between 865 and 785 cm^{-1} (typically at 830 cm^{-1}), which can be used to monitor the extent of reaction by measuring the decrease in intensity of the epoxide absorbance as cure proceeds. Gelation on a molecular level can be approximated as the point at which the resin begins to be insoluble.

In this paper the above mentioned techniques and thermogravimetric analysis (TGA) are used to characterize the cure of an epoxy/amine system, and the concept of a TTT cure diagram is used to generate a model of the cure behavior, which is quantitatively compared with the data.^{6,7}

Modeling the Cure Behavior

Gelation and Vitrification

Critical to an understanding of the "S"-shaped vitrification curve (Fig. 1) is the relationship between the glass transition temperature (T_g) and the extent of conversion at the glass transition (X_g). Complete analysis would take into account the reaction kinetics becoming diffusion-controlled on vitrification due to the increasing local viscosity which eventually quenches the reaction. According to the approach of Adabbo and Williams⁸ using Di Benedetto's equation,⁹ the glass transition temperature increases with increasing extent of conversion as follows:

$$\frac{T_g - T_{g0}}{T_{g0}} = \frac{(E_x/E_m - F_x/F_m)X_g}{1 - (1 - F_x/F_m)X_g} \quad (1)$$

where E_x/E_m is the ratio of lattice energies for crosslinked and uncrosslinked polymer and F_x/F_m is the corresponding ratio of segmental mobilities. The latter ratio is a measure of the mobility of the segment between crosslinks and therefore, is a function of the distance between crosslinks and hence $T_{g\infty}$. Experimental results for epoxy resins^{8,10} show that increasing the separation between crosslinks increases the ratio of segmental mobilities.

The ratio $(E_x/E_m)/(F_x/F_m)$ can be determined from measurement of the minimum and maximum glass transition temperatures since when $X_g = 0$ and 1 , $T_g = T_{g0}$ and $T_{g\infty}$, respectively, and, therefore, from eq. (1),

$$\frac{E_x/E_m}{F_x/F_m} = \frac{T_{g\infty}}{T_{g0}} \quad (2)$$

The ratios E_x/E_m and F_x/F_m in eqs. (1) and (2) can be determined by fitting eq. (1) to a plot of X_g vs. T_g .

Table I lists the values of these ratios, along with T_{g0} and $T_{g\infty}$, for several thermosetting systems whose extent of conversion vs. T_g data were found in the literature.^{3,11,12,13} Although T_{g0} and/or $T_{g\infty}$ had to be estimated for some of the systems, there is a good correlation between the experimental data and values calculated from eq. (1), which are represented by the lines in Figure 2.

The overall reaction rate is a function of the temperature, concentration of reactants, reaction mechanism, and the local microviscosity (which in turn is a

TABLE I
Lattice Energy Ratio and Segmental Mobility Ratio for Epoxy Systems

System	T_{g0} (°C)	T_{g-} (°C)	E_s/E_m	F_s/F_m	Reference
DGEBA/MDA ^a	-9 ^g	170	0.76	0.45	11
Epoxy/HHPA ^b	20(?) ^g	250 (?)	0.62	0.35	11
Epoxy glass laminate	62	127	0.84	0.71	12
Epon 828/DDS ^c	11 ^f	189	1.21	0.74	13
DGEBA/amine ^d	-10	115 (?)	0.62	0.41	3
Epon 828/PACM-20 ^e	-19	166	0.34	0.19	this work

^a Diglycidyl ether of Bisphenol A [Araldite F (CY 205) Ciba Geigy]/4,4'-methylene-dianiline.

^b Cyclo aliphatic epoxy (Araldite CY 175 Ciba Geigy)/hexahydrophthalic anhydride.

^c 4,4'-Diamino diphenyl sulfone.

^d 4,4'-Diamino-3,3'-dimethylcyclohexylmethane.

^e Bis(*p*-aminocyclohexyl)methane.

^f Unpublished data from this laboratory.

^g Values not given in literature for numbers followed by (?).

function of the molecular weight and temperature):

$$\frac{dX}{dt} = A \exp(-E_A/RT) f(X) / (\eta_L) \quad (3)$$

where X is the extent of reaction at time t , A is the kinetic Arrhenius factor, E_A is the activation energy, R is the molar gas constant, T is the temperature (K), $f(X)$ is a function of the reaction mechanism and the extent of conversion, and $f(\eta_L)$ is a function of the local viscosity. At each isothermal cure temperature below T_{g-} the reaction proceeds normally until the molecular weight increases to the extent that the glass transition approaches the cure temperature; the viscosity factor in eq. (3) becomes important as the material vitrifies.^{3,14,15}

In the absence of diffusion control the general kinetic equation which describes the reaction is

$$\frac{dX}{dt} = A \exp(-E_A/RT) f(X) \quad (4)$$

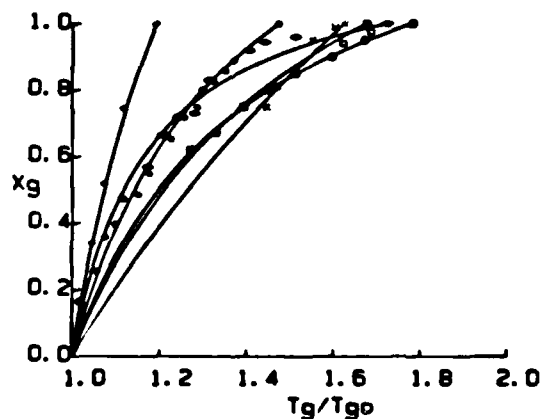


Fig. 2. Extent of conversion at vitrification vs. temperature for several epoxy systems: (□, ○) Fiach et al.¹¹; (+) Gray¹²; (×) Barton¹³; (•) Lunak et al.³; (◐) this work.

For a stoichiometric mixture of reactants the simplest expression for $f(X)$ is

$$f(X) = (1 - X)^n \quad (5)$$

where n is the order of reaction; or, for an autocatalytic reaction,

$$f(X) = (B + X^m)(1 - X)^n \quad (6)$$

where B is the ratio of rate constants, k_1/k_1' .¹⁶ If the kinetics of cure can be described by a single homogeneous reaction over the entire temperature range (T_{g0} to $T_{g\infty}$), the time to reach vitrification (i.e., T_g) during isothermal cure can be obtained by integrating eq. (4):

$$t_{vit}^* = \exp(Ar/T^*) \int_0^{X_g(T^*)} \frac{dX}{f(X)} \quad (7)$$

where $t_{vit}^* = At_{vit}$ is the dimensionless time to reach vitrification, $T^* = T/T_{g0}$ is a dimensionless temperature, and $Ar = E_A/RT_{g0}$ is the Arrhenius number. Rearranging eq. (1) to solve for X_g , the extent of conversion when the glass transition temperature is equal to the cure temperature,

$$X_g = \frac{T_g^* - 1}{E_x/E_m - 1 + (1 - F_x/F_m)T_g^*} \quad (8)$$

By substituting for X_g in eq. (7), the time to vitrification can be calculated. The time to reach gelation can also be calculated if the extent of conversion at gelation is known:

$$t_{gel}^* = \exp(Ar/T^*) \int_0^{X_{gel}} \frac{dX}{f(X)} \quad (9)$$

The integrations and times to gelation and vitrification as a function of reaction kinetics are tabulated in Table II.

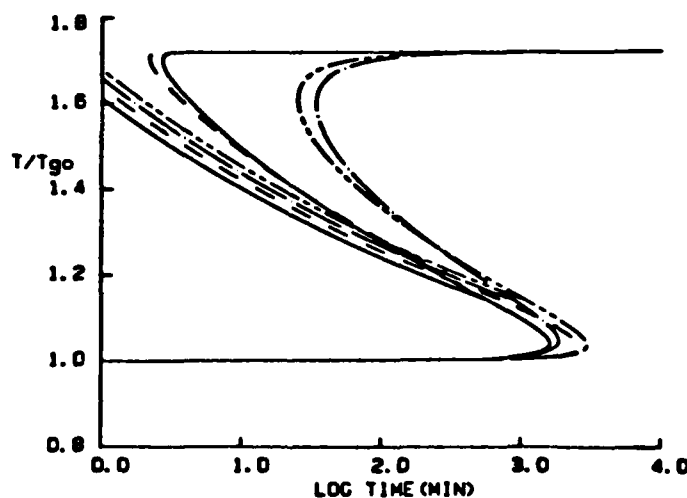


Fig. 3. Theoretical isothermal TTT cure diagrams, generated using eqs. (9) and (7) for first (—) and second (---) order kinetics, and autocatalyzed first (- · -) and autocatalyzed second (· · ·) order kinetics. The following parameters anticipate experimental results for Epon 828/PACM-20: $E_x/E_m = 0.34$, $F_x/F_m = 0.19$, $X_{gel} = 0.75$, $T_{g0} = 254^\circ\text{K}$, $T_{g\infty} = 439^\circ\text{K}$, $A = 4.5 \times 10^6 \text{ min}^{-1}$, and $Ar = 25$. For simplicity, $B (= k_1/k_1')$ is $1/2$ and so is independent of temperature, and $m = 1$; also the numerical value of the rate constant found for first order kinetics is used for the other cases.

TABLE II
Theoretical Time to Gel and Time to Vittrification for Various Reaction Kinetics^a

Reaction kinetics	$f(X)$	$\int_0^X \frac{dX}{f(X)}$	t_m	t_{gel}
Zero order	1	X	$e^{A_0/T^0} \left(\frac{T^0 - 1}{E - 1 + (1 - F)T^0} \right)$	$e^{A_0/T^0} (X_{gel})$
First order	$1 - X$	$-\ln(1 - X)$	$-e^{A_0/T^0} \ln \left(\frac{E - FT^0}{E - 1 + (1 - F)T^0} \right)$	$-e^{A_0/T^0} \ln(1 - X_{gel})$
Second order	$(1 - X)^2$	$\frac{X}{1 - X}$	$e^{A_0/T^0} \left(\frac{T^0 - 1}{E - FT^0} \right)$	$e^{A_0/T^0} \frac{X_{gel}}{1 - X_{gel}}$
Autocatalytic first order	$(B + X)(1 - X)$	$\frac{\ln \left[\frac{X + B}{B(1 - X)} \right]}{(1 + B) \left[B(1 - X) \right]}$	$\frac{e^{A_0/T^0} \ln \left[\frac{(T^0 - 1)/B + E - 1 + (1 - F)T^0}{E - FT^0} \right]}{(1 + B) \left[\frac{(T^0 - 1)/B + E - 1 + (1 - F)T^0}{E - FT^0} \right]}$	$\frac{e^{A_0/T^0} \ln \left[\frac{X_{gel} + B}{B(1 - X_{gel})} \right]}{(1 + B) \left[B(1 - X_{gel}) \right]}$
Autocatalytic second order	$(B + X)(1 - X)^2$	$\frac{1}{(1 + B) \left[1 - X \right]} + \frac{\ln \left[\frac{X + B}{B(1 - X)} \right]}{(1 + B) \left[B(1 - X) \right]}$	$\frac{e^{A_0/T^0} \left(\frac{T^0 - 1}{E - FT^0} \right)}{(1 + B) \left[\frac{(T^0 - 1)/B + E - 1 + (1 - F)T^0}{E - FT^0} \right]} + \frac{\ln \left[\frac{(T^0 - 1)/B + E - 1 + (1 - F)T^0}{E - FT^0} \right]}{(1 + B) \left[\frac{(T^0 - 1)/B + E - 1 + (1 - F)T^0}{E - FT^0} \right]}$	$\frac{e^{A_0/T^0} \left(\frac{X_{gel}}{1 - X_{gel}} \right)}{(1 + B) \left[1 - X_{gel} \right]} + \frac{\ln \left[\frac{X_{gel} + B}{B(1 - X_{gel})} \right]}{(1 + B) \left[B(1 - X_{gel}) \right]}$

^a $E = E_s/E_m$, $F = F_s/F_m$.

By definition, $_{\text{gel}}T_g$ is the temperature at which the time to gel and the time to vitrify are the same. It follows that $_{\text{gel}}T_g$ is the glass transition of the system at its gel point. By evaluating eq. (1) at $X_g = X_{\text{gel}}$, $_{\text{gel}}T_g$ can be calculated:

$$_{\text{gel}}T_g = \frac{1 + (E_x/E_m - 1)X_{\text{gel}}}{1 + (F_x/F_m - 1)X_{\text{gel}}} \quad (10)$$

which implies that $_{\text{gel}}T_g$ is independent of the reaction kinetics.

Using eqs. (7) and (9), the theoretical TTT cure diagram for a typical amine-cured epoxy system is presented in Figure 3 for first-order, second-order, and autocatalytic reaction kinetics. This model exhibits the same features as the conceptual diagram in Figure 1: the vitrification curve is "S"-shaped, with a minimum time to vitrify at high temperatures (near $T_{g\infty}$) and a maximum time to vitrify at low temperatures (near T_{g0}), and the gelation curve crosses the vitrification curve at a characteristic temperature $_{\text{gel}}T_g$. The shape of the curve is a function of the kinetics as well as the physical property parameters T_{g0} , $_{\text{gel}}T_g$, and $T_{g\infty}$, and the relationship between the glass transition temperature and the conversion at T_g . A system which cures according to a first-order mechanism gels and vitrifies more rapidly, and has a more abrupt turn around at the minimum time to vitrify than one which cures according to a second-order mechanism. An effect of an autocatalytic mechanism is to decrease the minimum time to vitrification above $_{\text{gel}}T_g$ and to increase the maximum time to vitrification below $_{\text{gel}}T_g$. Autocatalysis retards gelation for the cases considered.

Viscosity as a Function of Cure

The zero shear bulk viscosity of a curing resin is directly proportional to the weight average molecular weight \bar{M}_w below the critical molecular weight for chain entanglement,¹⁷⁻¹⁹ i.e.,

$$\eta = K\bar{M}_w \quad (11)$$

where K is a constant incorporating an Arrhenius viscosity-temperature relationship^{14,19,20}

$$K = \eta_{\infty} \exp(E_a/RT) \quad (12)$$

in which η_{∞} is the extrapolated viscosity at $T = \infty$ and E_a is the activation energy.

Near the glass transition the viscosity-temperature relationship is no longer Arrhenius but is modified by the WLF equation²¹

$$\ln \frac{\eta}{\eta_{T_0}} = \frac{-C_1(T - T_0)}{C_2 + T - T_0} \quad (13)$$

where C_1 , C_2 , and T_0 are constants chosen to fit the viscosity-temperature data near the glass transition and to match the Arrhenius relationship [eq. (12)] at the reference temperature T_0 . Substituting eq. (12) into eq. (11) and then combining it with eq. (13) results in the following relationship:

$$\ln \eta = \ln \eta_{\infty} + \ln \bar{M}_w + \frac{E_a}{RT_0} - \frac{C_1(T - T_0)}{C_2 + T - T_0} \quad (14)$$

where $T_0 = 50 + T_g$ when $T < 50 + T_g$, and $T_0 = T$ when $T \geq 50 + T_g$. The

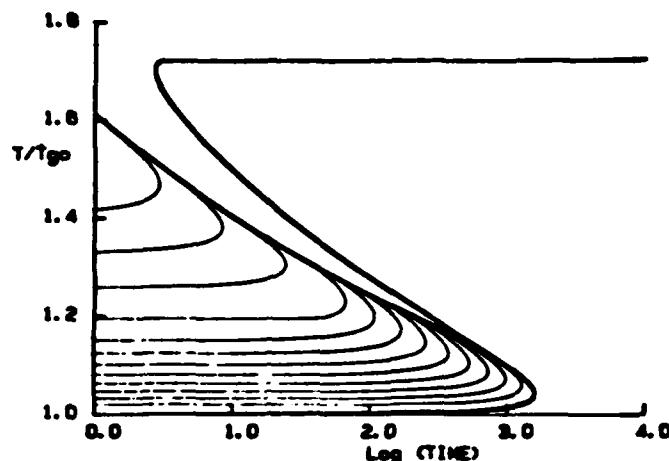


Fig. 4. Calculated times to attain specific zero shear rate viscosities at various isothermal cure temperatures using the time-temperature-viscosity relationships [Eqs. (14), (15), (4), (8)] for first-order kinetics. Successive contour lines differ by a factor of 10. The curves approach the computed gelation curve above $_{gel}T_g$ and the vitrification curve below $_{gel}T_g$ (Fig. 20).

reference temperature, $T_g + 50$, is arbitrarily chosen to be the temperature above which the viscosity-temperature relationship is Arrhenius. In order to calculate the viscosity of a system while it is curing isothermally, three other relationships are required:

(1) The relation between the weight average molecular weight and extent of reaction, which has been derived by Macosko and Miller for nonlinear step-growth polymers for cases of equal²² as well as unequal reactivity²³ of reactive species. For a stoichiometric mixture of a difunctional epoxy and a tetrafunctional amine (assuming equal reactivity of the primary and secondary amine hydrogens) the equation reduces to

$$\bar{M}_w = \frac{\frac{1}{2}M_A^2(1 + X^2) + M_E^2(1 + 3X^2) + 4M_A M_E X}{(\frac{1}{2}M_A + M_E)(1 - 3X^2)} \quad (15)$$

where M_A and M_E are the molecular weights of the amine and epoxy monomers, respectively, and X is again the extent of reaction.

(2) The relation between extent of reaction and time, which requires integration of the kinetic rate equation [eq. (4)].

(3) The relation between extent of conversion and the glass transition, which has already been introduced [eq. (1)].

The time required to reach a specified viscosity during isothermal cure can be calculated using eqs. (14), (15), (4), (8), and Table II. Isoviscosity contours are plotted on a time-temperature plot (Fig. 4) along with the gelation and vitrification curves for a first order epoxy/amine reaction using the parameters and physical constants listed for Epon 828/PACM-20 in Table III. As the glass transition (vitrification) is approached, the space between successive contour lines decreases more rapidly than for Arrhenius type behavior. Another feature of this figure is the way in which the contour lines all converge to the gelation line where the weight average molecular weight becomes infinite. This is in contrast to other models,^{14,20} in which gelation was not accounted for in the calculation of rheological properties.

TABLE III
Physical Constants and Other Parameters Used in Viscosity Calculations (Fig. 4)

Parameter	Symbol	Value	Source
Molecular weight (amine) (g/mol)	M_A	210	
Molecular weight (epoxy) (g/mol)	M_E	382	
Functionality (of amine)	f	4	
T_g of uncured resin ($^{\circ}\text{C}$)	T_{g0}	-19	this work
T_g of fully cured resin ($^{\circ}\text{C}$)	$T_{g\infty}$	165	this work
Ratio of lattice energy (crosslinked/monomer)	E_r/E_m	0.337	this work
Ratio of segmental mobility (crosslinked/monomer)	F_r/F_m	0.194	this work
Extent of conversion at gelation	X_{gel}	0.57	Ref. 2
WLF, equation constant	C_1	11	fit
WLF, equation constant ($^{\circ}\text{K}$)	C_2	75	fit
Universal gas constant (cal/mol $\cdot^{\circ}\text{K}$)	R	1.987	
Kinetic activation energy (cal/mol)	E_A	12,618	this work
Kinetic Arrhenius factor (min $^{-1}$)	A	4.51×10^6	this work
Viscosity activation energy (cal/mol)	E_v	27,300	Ref. 20
Viscosity Arrhenius factor (Pa-s-mol/g)	η_{∞}	6.25×10^{-13}	Ref. 20

EXPERIMENTAL

Materials

The thermosetting resin investigated was a stoichiometric mixture (1 epoxy/1 amine hydrogen) of a diglycidyl ether of Bisphenol A (Shell Epon 828) and bis(*p*-aminocyclohexyl) methane (PACM-20: DuPont) used as received. Epon 828 is a viscous liquid at room temperature with an equivalent molecular weight of 191 g/mol epoxide, and PACM-20 is a liquid (mp 15°C) with an equivalent molecular weight of 52.5 g/mol amine hydrogen. After mixing the viscous solution ($T_{g0} = -19^{\circ}\text{C}$) at room temperature with an electric stirrer, the master batch was separated into small vials which were stored in liquid nitrogen. For each experiment a separate vial was allowed to warm to room temperature before it was opened (to prevent water from condensing on the resin). Except for the gel fraction experiment, in which there was an additional degassing step (20 min, 25°C), the elapsed time from taking each vial out of the liquid nitrogen to the start of the experiment was the same (30 min) so as to synchronize the experiments using the different techniques.

EXPERIMENTAL PROCEDURES AND RESULTS

Torsional Braid Analysis (TBA)

Each TBA specimen was made by dipping a multifilamented glass braid into the epoxy resin and smoothing it between two pieces of paper to remove excess. It was then mounted in the sample chamber at the temperature of cure in a helium atmosphere and the modulus and logarithmic decrement at about 1 Hz were monitored as a function of time by an automated apparatus (Plastics Analysis Instruments, Inc., P.O. Box 408, Princeton, NJ 08540).^{1,24} At each isothermal temperature the specimen was cured until the reaction was either complete or quenched, as indicated by a leveling off of the modulus. Typically, three peaks in logarithmic decrement were observed during cure, which were identified as an isoviscous pregel phenomenon, a liquid-to-rubber transformation (gelation),

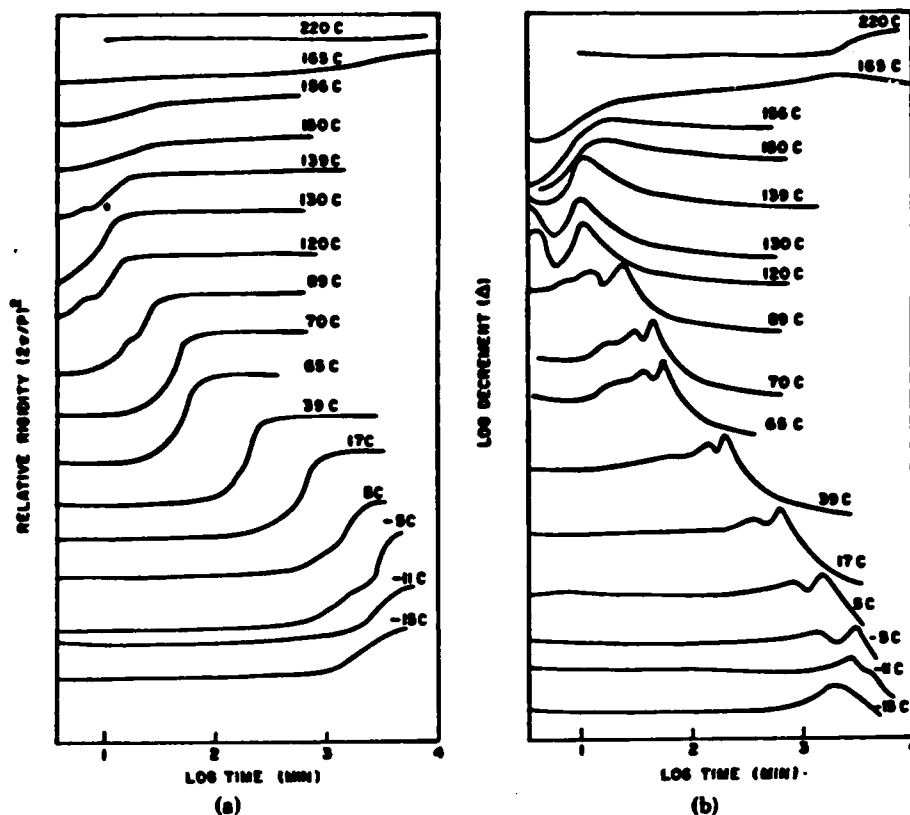


Fig. 5. TBA spectra during isothermal cure of Epon 828/PACM-20 from -15°C to 220°C : (a) relative rigidity; (b) logarithmic decrement.

and vitrification, respectively.^{1,4} Representative spectra are shown in Figures 5(a) and 5(b), and the times to these events are included in Table IV. Dynamic mechanical spectra were then obtained by cooling (at $1.5^{\circ}\text{C}/\text{min}$) to -190°C and then heating (at the same rate) to 200°C . If the resin was only partially cured during the isothermal stage, heating the resin to 200°C completes the cure (T_{g-} is 165°C). A subsequent scan from 200°C to -190°C provides the spectrum of the fully cured resin in which three relaxations are observed: the glass transition (T_g), a secondary sub-glass transition (T_{sec}) related to the motion of the $-\text{CH}_2-\text{CH}(\text{OH})-\text{CH}_2\text{O}-$ group in the epoxy^{25,26} and a cryogenic relaxation below T_{sec} .²⁶ The values of T_{sec} , T_{sec-} , T_g , and T_{g-} obtained from these scans are also included in Table IV and plotted in Figure 6. Both T_{sec} and T_g increase with increasing extent of cure (higher isothermal cure temperature), and decrease upon degradation (above 220°C). The cryogenic relaxation decreases in intensity with increasing cure.

As representative examples of the dynamic mechanical spectra of the partially cured resin after extended isothermal cure, temperature scans after isothermal cure at 5°C (i.e., below $_{gel}T_g$) and after isothermal cure at 89°C (i.e., between $_{gel}T_g$ and T_{g-}) are shown in Figures 7(a) and 7(b), respectively. The plots also include the temperature scans of the fully cured materials. As the scan reaches tem-

TABLE IV
Time to Pregel, Time to Liquid-to-Rubber, and Time to Vittrification Events, vs. Cure Temperature (TBA data); Also: T_{sec} and T_g Data after Extended Isothermal Cure

T_{cure} (°C)	t_{pregel} (min)	$t_{liquid-to-rubber}$ (min)	t_{vit} (min)	T_{sec} (°C)	T_{sec-} (°C)	T_g (°C)	T_{g-} (°C)
260					-56		170
240					-50		149
220					-46		151
197					-29	166	159
165			2377		-28	171	164
161			2177		-30	169	169
158			238		—	162	—
156			20		—	162	165
150			16		-32	162	165
139			11		-31	161	163
130			10		-31	158	165
120			11	-34	-30	155	164
110		6	14	-41	-28	130	167
89		12	24	-49	-27	117	165
70	18	30	46	-55	-28	100	165
65	24	38	57	-56	-29	—	167
39	64	141	203	-60	-30	67	162
17	189	375	641	-64	-30	40	164
5	340	820	1544	-62	-32	—	158
-5		1223	2948	-63	-28	4	169
-11			2891	-70	-33	-2	162
-15			1947	-74	-30	-12	162
Uncured				-80	—	-19	

peratures above the temperature of cure, the extent of cure changes during measurement. The temperature scan (-190°C to 200°C) of the material cured at 5°C displays six loss peaks [Fig. 7(a)] which are designated $T_{cryogenic}$, T_{sec} , T_g , T_R , revitrification, and devitrification (T_{g-}) in order of increasing temperature. The T_R loss peak arises when the temperature scan rate equals the glass tran-

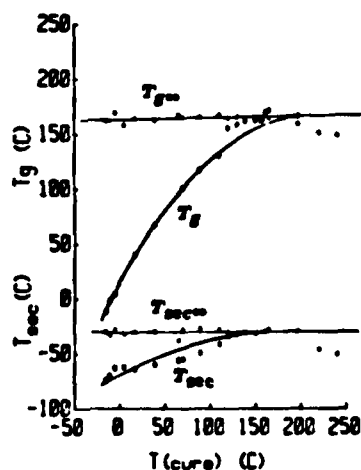


Fig. 6. T_{sec} (•) and T_g (•) as a function of the cure temperature of Epon 828/PACM-20, and T_{sec-} (+) and T_{g-} (+) after heating to 200°C .

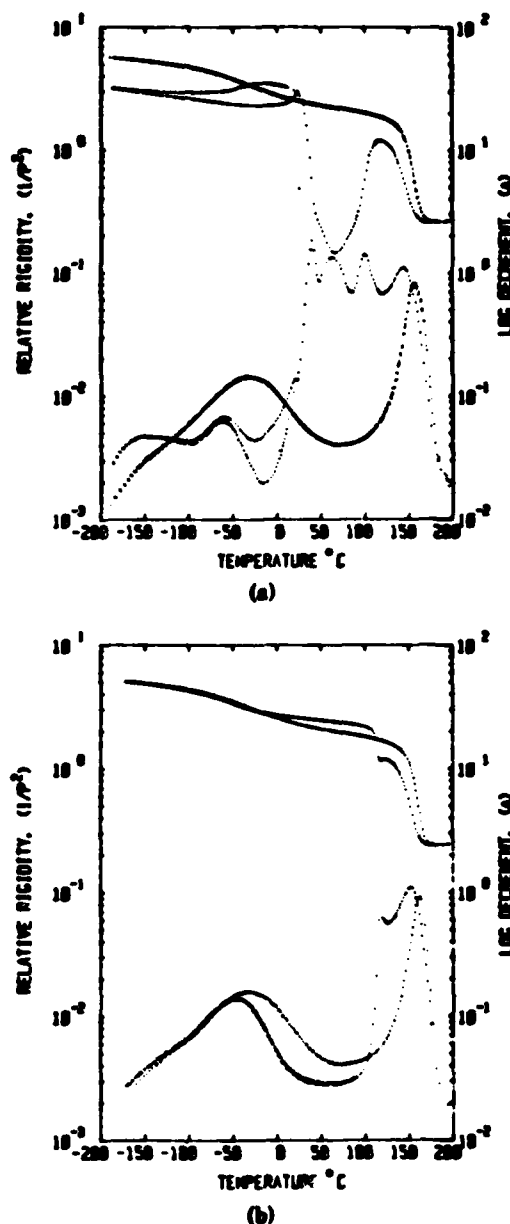


Fig. 7. (a) TBA spectra after isothermal cure at 5°C of Epon 828/PACM-20: 5 → -190 → 200 → -190°C (1.5°C/min). Compare the behavior of the uncured material (which displays six loss peaks) with that of the fully cured material (which displays two distinct loss peaks). (b) TBA spectra after isothermal cure at 89°C of Epon 828/PACM-20: 89 → -190 → 200 → -190°C (1.5°C/min). Compare the behavior of the uncured and fully cured materials which display three and two distinct loss peaks, respectively.

sition temperature's rate of increase.^{27,28} The spectrum of the material cured isothermally above $_{gr}T_g$ [Fig. 7(b)] differs from that cured below $_{gr}T_g$ [Fig. 7(a)] in the following respects: the temperature window between T_g and revitrification is narrower; there is no hysteresis between cooling and heating in the glassy

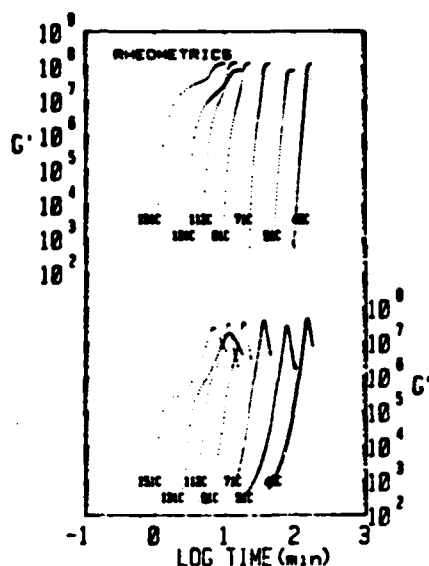


Fig. 8. RDS spectra during isothermal cure from 42°C to 151°C of Epon 828/PACM-20: Top: Dynamic shear modulus; bottom: dynamic loss modulus.

state (which is a consequence of the higher molecular weight); and the pattern for the two glassy state relaxations is closer to that of the fully cured material.

The modulus between T_{sec} and T_g of the partially cured material is greater than that of the fully cured material. Similar results have been obtained for other systems.^{25,1} This has been associated with a decrease in density in the glassy state and an increase in equilibrium moisture content with increasing extent of cure.^{29,30}

Rheometrics Dynamic Spectrometer (RDS)

Dynamic viscosity η^* , elastic modulus G' , and loss modulus G'' were obtained from oscillatory shear measurements at 1.6 Hz as a function of time at various temperatures using parallel plates (25 mm diameter) separated by a 0.5 mm gap. (The sample chamber had been preheated to the cure temperature and was purged with nitrogen.) In the fluid state the maximum deformation was 5%; as the modulus increased, the deformation was decreased so as to keep the torque from going off scale. The G' and G'' data are shown in Figure 8, and the times

TABLE V
Time to Liquid-to-Rubber and Time to Vitrification Events (RDS Data)

T_{cure} (°C)	$t_{liquid-to-rubber}$ (min)	t_{vit} (min)
151	1.8	7
133	4.3	12
112	6.8	11
92	12.3	18
71	27.2	25
51	—	76
42	—	149

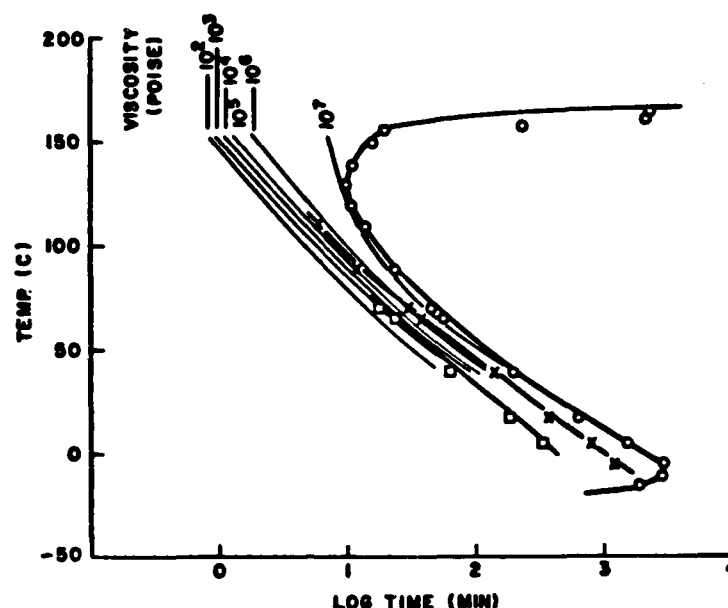


Fig. 9. Isoviscosity (dynamic) contours (RDS data); also TBA pregel (\square), liquid-to-rubber (\times), and vitrification (\circ) events.

to the liquid-to-rubber transformation and vitrification, obtained from the shoulder and peak, respectively, in the G'' data, are tabulated in Table V.

The dynamic viscosity is plotted as isoviscosity contours in Figure 9. Also plotted are the times to the three events observed in the TBA data: the first event occurs at approximately the same viscosity¹ (>1000 P) over the common temperature range in which it was observed, whereas the second event cuts across the isoviscosity contours above 50°C .

Infrared Spectroscopy (FT-IR)

Infrared spectra from 4000 to 400 cm^{-1} were collected using an FT-IR spectrometer (Nicolet 7199), equipped with a liquid nitrogen cooled detector (HgCdTe) and a temperature programmer (Tetrahedron Wizard). Spectra were averaged over 32 scans taken at 4 cm^{-1} resolution. A drop of uncured resin was sandwiched between two NaCl plates which were then placed in a temperature-controlled cell (Wilkes). The spectrometer was continuously purged with nitrogen. A series of spectra was obtained at each temperature, at temperatures ranging from 25 to 150°C .

A typical spectrum of uncured Epon 828/PACM-20 taken at room temperature is shown in Figure 10. The extent of reaction at any time can be related to the ratio of the area of the epoxide peak at 915 cm^{-1} to its initial area. To eliminate error due to sample slippage, etc., the epoxide peak can be normalized by dividing its area by that of a reference peak (1184 cm^{-1}). The 1184 cm^{-1} peak, due to C—C stretching of the bridge carbon atom between the two *p*-phenylene groups,³¹ is the preferred choice over the aromatic bands at 1607 and 1501 cm^{-1} due to the interference of the latter with the changing primary and secondary

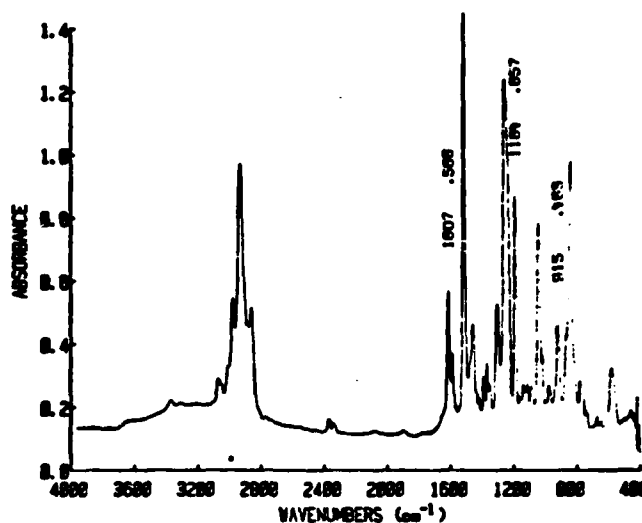


Fig. 10. FTIR spectrum of Epon 828/PACM-20: 4000 cm^{-1} to 400 cm^{-1} .

amine bands at 1625 and 1508 cm^{-1} , respectively. Therefore,

$$1 - X = A_{\text{epoxy}}(t) = \frac{A_{915}(t) A_{1184}(0)}{A_{1184}(t) A_{915}(0)} \quad (16)$$

where $A_{915}(t)$ is the absorbance at 915 cm^{-1} at time t , $A_{1184}(t)$ is the absorbance at 1184 cm^{-1} at time t , $A_{\text{epoxy}}(t)$ is the fraction of unreacted epoxy at time t , and X is the extent of reaction with respect to epoxy.

The extent of conversion with respect to the epoxide group [as calculated in eq. (16)] is plotted in Figure 11 for several cure temperatures. At temperatures below 150°C the reaction is quenched by vitrification before it can reach completion. By plotting the extent of reaction as if it obeyed first-order reaction kinetics [$n = 1$ in eq. (5)] the apparent rate constant can be calculated from the slope of the linear portion (Fig. 12). The rate constants, the times at which the data deviate from a straight line (which was found to correspond to the vitrifi-

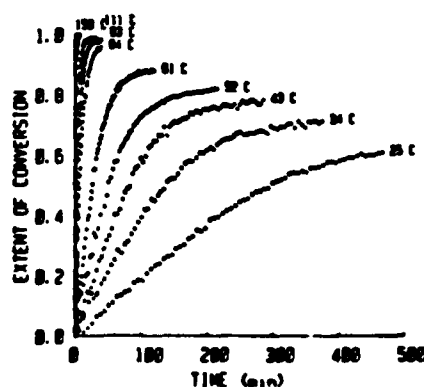


Fig. 11. Extent of conversion (IR) versus time during isothermal cure for Epon 828/PACM-20 from 25 to 150°C.

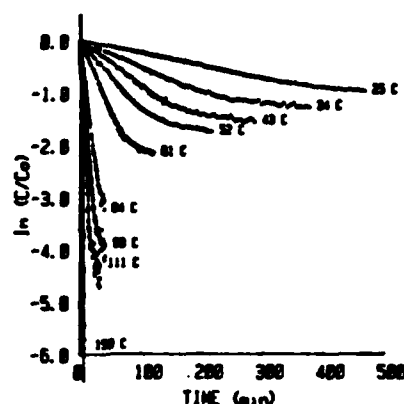


Fig. 12. Extent of conversion data (Fig. 11) plotted as first order kinetics. The slope of the linear portion is equal to the rate constant (see Table VI).

cation times), the times to vitrification, and the fractional conversion at vitrification (obtained from comparison of the isothermal extent of conversion data and the time to vitrification data) are tabulated in Table VI.

Gel Fraction

Small amounts (1–2 mL) of uncured resin were placed in ampules, degassed at 1 torr for 20 min (until the bubbles disappeared), sealed in a helium atmosphere, and placed in a heated oil bath held at a fixed temperature. The ampules were removed at selected intervals, quenched in liquid nitrogen, broken, and the soluble portion was extracted with dichloromethane for 3 h using a Soxhlet extraction column with coarse thimbles. The insoluble portion (gel) was then dried, weighed, and compared to the initial weight (before extraction) to give a gel fraction. This procedure was carried out with 10 samples at each of six cure temperatures ranging from 40°C to 90°C.

TABLE VI
Rate Constants, Times to Deviation from First Order Kinetics, Times to Vitrification, and Extents of Conversion at Vitrification vs. Temperature

T_{cure} (°C)	Rate constant ^a (min ⁻¹)	$t_{\text{deviation}}^b$ (min)	t_{vit}^b (min)	X_g^a
150	1.23	—	16	—
111	0.275	15	13	0.96
93	0.151	21	20	0.94
84	0.0951	28	27	0.92
61	0.0268	60	68	0.83
52	0.0136	93	103	0.73
43	0.00868	152	167	0.72
34	0.00465	251	244	0.67
25	0.00231	384	386	0.57

^a IR data (see Fig. 12).

^b TBA data (see Fig. 16).

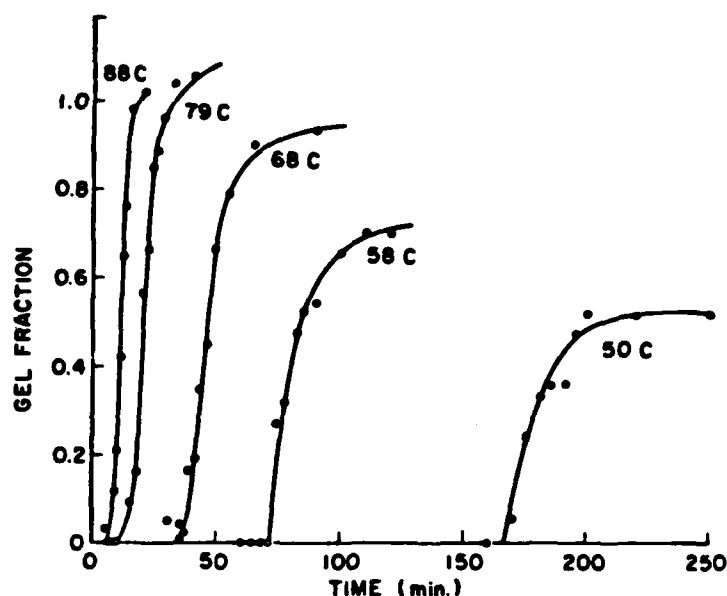


Fig. 13. Gel fraction versus time during isothermal cure for Epon 828/PACM-20 from 50°C to 88°C.

The gel fraction is plotted in Figure 13 as a function of time for several temperatures, and the gel points (defined as the onset of insolubility) are tabulated in Table VII.

Thermogravimetry (TGA)

Uncured samples were run at 5°C/min as well as isothermally at 225°C and 250°C under a nitrogen atmosphere in a DuPont 950 TGA. Figure 14 indicates that weight loss begins in the vicinity of 285°C at a scan rate of 5°C/min. Isothermally at 225°C 1% was lost after 10 h, and at 250°C 1% was lost after 5 h.

DISCUSSION

The TBA and RDS data provide the basis for generating a TTT cure diagram. The times to the liquid-to-rubber transformation and vitrification are plotted in Figure 15 as a function of the reduced isothermal cure temperature: except for the RDS vitrification data at $T^* = 1.66$ (150°C), the TBA and RDS data are consistent above gel T_g [$_{gel}T_g^* = 1.27$ (49°C)]. The shoulder in G'' of the RDS

TABLE VII
Times to Gel at Various Temperatures (Gel Fraction Data)

T_{cure} (°C)	t_{gel} (min)
88	9
79	13
68	38
58	72
50	165
40	no gel

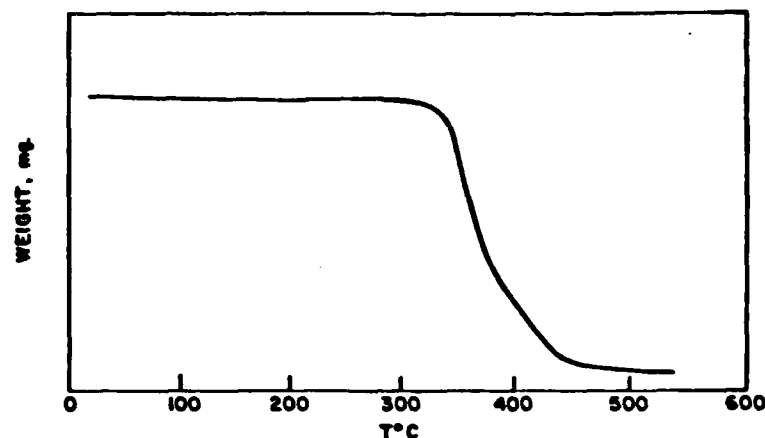


Fig. 14. Thermogravimetry scan of uncured Epon 828/PACM-20 at 5°C/min in nitrogen atmosphere.

data (Fig. 8) vanishes as the cure temperature decreases to $_{gel}T_g$, but the corresponding TBA peak persists at lower temperatures.¹ In addition, the times at which the kinetics begin to deviate from first order kinetics (Table VI) are also plotted in Figure 15 (designated "diffusion"): the fact that they lie on the "S"-shaped vitrification curve, determined by the peak in the logarithmic decrement (TBA), indicates that the reaction proceeds normally until the system vitrifies, i.e., there is no change in reaction mechanism or apparent rate constant at gelation,³² but the reaction becomes diffusion-controlled as it vitrifies.

The events identified as the liquid-to-rubber transformation can be correlated with molecular gelation by the gel fraction experiments. In Figure 16 these gel times (Table VII) have been included on the TTT diagram consisting of the TBA and RDS data. In Figure 17 the Arrhenius plot of rate constants determined by infrared (Table VI) is compared with the time-to-gel data obtained by gel

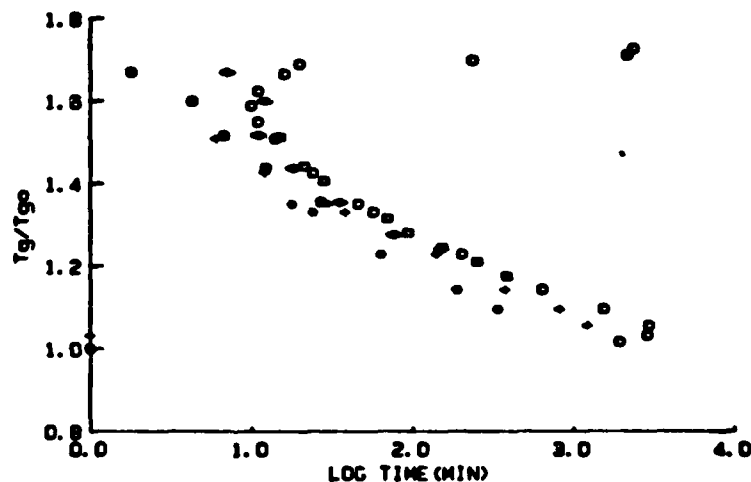


Fig. 15. TTT diagram of Epon 828/PACM-20: TBA, RDS, and IR data. TBA: (○) vitrification; (+) liquid-to-rubber; (•) pregel. RDS: (◐) vitrification; (◑) liquid-to-rubber. IR: (◻) diffusion.

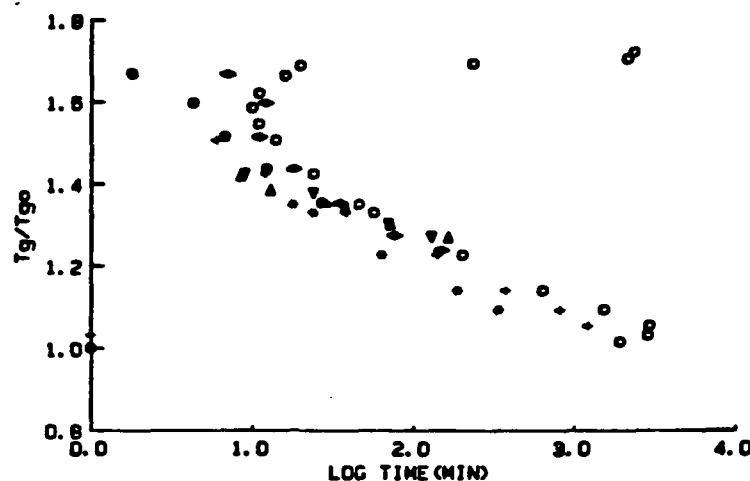


Fig. 16. TTT diagram of Epon 828/PACM-20: TBA, RDS, and gel fraction data. TBA: (○) vitrification; (+) liquid-to-rubber; (*) pregel. RDS: (◐) vitrification; (●) liquid-to-rubber. Gel fraction: (▽, △) helium.

fraction, TBA, and RDS experiments. The activation energies, obtained independently by each of these techniques, are listed in Table VIII. In the Epon 828/PACM-20 system the correlation is not as good as for other systems (see Appendix).

Since the material gels at 50°C but not at 41°C, $_{gel}T_g$ lies between 41°C and 50°C.

The extent of reaction at gelation can be determined by plotting the times to gel on a plot of extent of conversion contours. In Figure 18 it is seen that gelation occurs between 70% and 80% conversion over the entire temperature range. According to a statistical approach by Flory^{2,33} the critical extent of reaction at the gel point (X_{gel}) is

$$X_{gel} = 1/[r + r\rho(f - 2)]^{1/2} \quad (17)$$

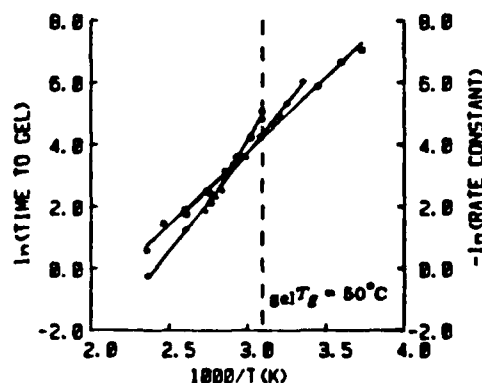


Fig. 17. Arrhenius plots of IR rate constants, gel times (gel fraction data), and times to liquid-to-rubber transformation (TBA and RDS data) for Epon 828/PACM-20. Activation energy (kcal/mol): (*) 16.8 (gel fraction); (+) 12.6 (FT-IR); (○) 10.7 (TBA); (□) 9.3 (RDS).

TABLE VIII
Comparison of Activation Energy Using Various Techniques

Technique	E_A (kcal/mol)	A^* (min^{-1})
IR	12.6	4.51×10^6
Gel fraction	16.8	
TBA	10.7	
RDS	9.3	

* Arrhenius factor determined from intercept of Arrhenius plot (Fig. 17).

where r is the ratio of epoxide to amine hydrogen, ρ is the fraction of amine hydrogen that is part of a multifunctional reactant ($f > 2$), and f is the functionality of the branching units. For the Epon 828/PACM-20 system, $r = \rho = 1$ and $f = 4$, so

$$X_{\text{gel}} = 1/[1 + (4 - 2)]^{1/2} \quad (18)$$

The discrepancy between the experimental (0.7–0.8) and theoretical (0.57) values for X_{gel} may be attributed to the unequal reactivity of the primary and secondary amines. There is spectroscopic evidence³⁴ which suggests that, although the amine-epoxide reaction predominates prior to gelation, only approximately half of the secondary amine hydrogens have reacted by the time all of the epoxides have reacted. This implies that a second crosslinking reaction mechanism is operative, presumably epoxide-epoxide or hydroxyl-epoxide.

COMPARISON OF THE MODEL AND EXPERIMENTAL DATA

The relationship between the extent of conversion at vitrification and the glass transition temperature is the basis of the TTT cure diagram because when it is coupled with the reaction kinetics it can be used to generate the "S"-shaped vitrification curve. The extent of conversion at the time of vitrification was

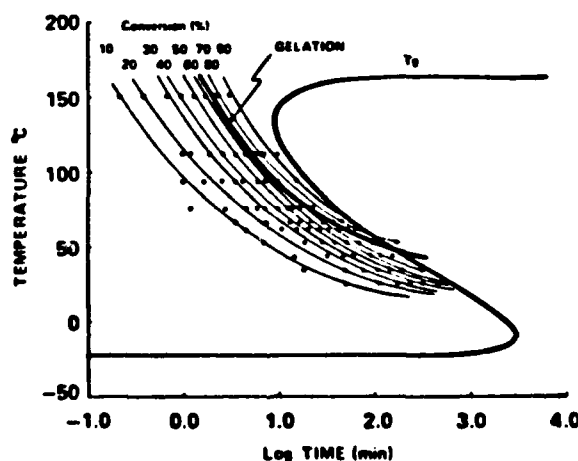


Fig. 18. Extent of isoconversion contours, gel fraction data, and times to vitrification data (T_g) for Epon 828/PACM-20. The extent of conversion at gelation is between 70% and 80%.

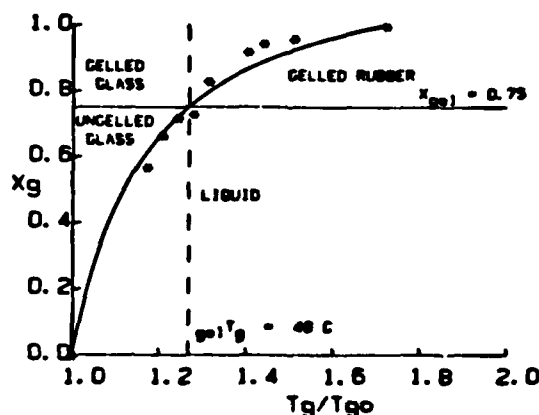


Fig. 19. Extent of conversion at vitrification as a function of temperature for Epon 828/PACM-20. Line is best fit of data (Table VI) to eq. (8).

obtained from the IR data at each cure temperature, interpolating the times to vitrification from the TBA data (Table IV and Fig. 15). The curve in Figure 19 defines the extent of conversion at vitrification: it is a fit of eq. (8) to the extent of conversion at vitrification vs. temperature data. Below the curve the material is liquid or gelled rubber; above the curve the material is ungelled glass or gelled glass.

The parameters found from a nonlinear least squares fit³⁵ of the data gave values of $E_x/E_m = 0.34$ and $F_x/F_m = 0.19$ for the relative mobility and lattice energies of the segments between crosslinks, respectively.

Although Di Benedetto estimated $E_x/E_m = 1.2$ for the styrene-divinyl-benzene system,⁹ and Williams assumed it to be unity for most thermosets,⁸ there is no *a priori* reason for it to be limited to these values, since it can be approximated by⁹

$$\frac{E_x}{E_m} \approx \frac{d_m}{d_x} \frac{(M_0)_x}{(M_0)_m} \left(\frac{\delta_x}{\delta_m} \right)^2, \quad (19)$$

where d_m and d_x are the densities, $(M_0)_m$ and $(M_0)_x$ are the monomer unit molecular weights, and δ_m and δ_x are the solubility parameters of uncrosslinked and crosslinked polymer, respectively. The values of E_x/E_m found for Epon 828/PACM-20 and the systems listed in Table I tend to be less than 1, suggesting that $d_m/d_x < 1$ and/or $\delta_x/\delta_m < 1$. According to Nielsen, the ratio F_x/F_m is expected to be zero, whereas Williams found it to be approximately 0.7 for several thermosets. The present analysis, which utilizes both ratios, finds that values of F_x/F_m range between 0.19 and 0.7. Using the values of the ratios of lattice energies and segmental mobilities obtained for Epon 828/PACM-20 in eq. 10, $_{gel}T_g$ is 49°C for $X_{gel} = 0.75$.

Figure 20 is the experimentally determined TTT cure diagram, with data from TBA, RDS, gel fraction, and IR experiments, on which have been superimposed the theoretical "S"-shaped vitrification and gelation curves for first-order kinetics with gelation at 75% conversion.

Below $T^* \approx 1.4$ (85°C) the gelation and vitrification curves show excellent agreement with the data. On comparing the upper portion of the vitrification

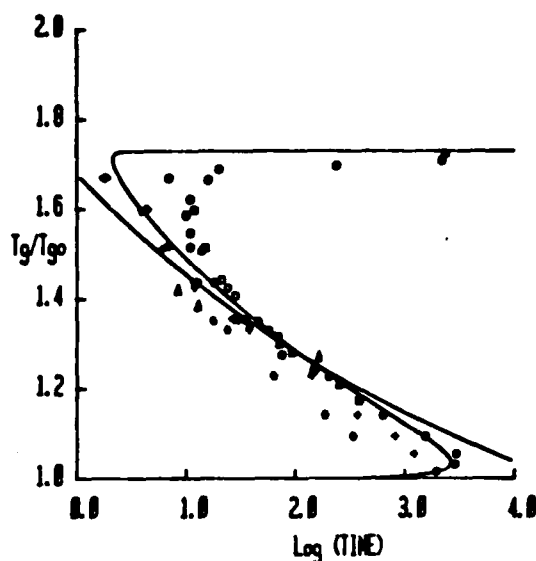


Fig. 20. Isothermal TTT cure diagram for Epon 828/PACM-20. Theoretical (solid lines): First-order kinetics using the following parameters: $T_{g0} = -19^{\circ}\text{C}$, $T_{g\infty} = 166^{\circ}\text{C}$, $E_s/E_m = 0.34$, $F_s/F_m = 0.19$, $E_A = 12.6 \text{ kcal/mol}$, $A = 4.5 \times 10^5 \text{ min}^{-1}$, $X_{g0} = 0.75$, and $_{g0}T_g = 49^{\circ}\text{C}$. Experimental: (•) pregel (TBA); (+) liquid-to-rubber (TBA); (O) vitrification (TBA); (◐) liquid-to-rubber (RDS); (●) vitrification (RDS); (◻) diffusion control (IR); (Δ) gelation (gel fraction).

curve to the second-order kinetics curve in Figure 3, it appears that the reaction mechanism changes from first to second order in the vicinity of 90°C with a corresponding shift in the gelation curve as well. [Since this is in the center of

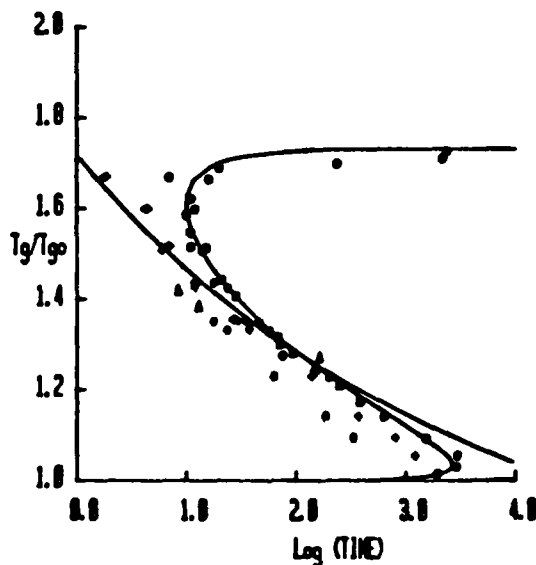


Fig. 21. Isothermal TTT cure diagram for Epon 828/PACM-20. Theoretical (solid lines): $T^* < 1.3$: $t = t$ (first order); $1.3 < T^* < 2.3$: $t = [1 - (T^* - T_L^*)/(T_U^* - T_L^*)] t$ (first order) + $[(T^* - T_L^*)/(T_U^* - T_L^*)] t$ (second order); T_U^* = temperature above which reaction is second order, T_L^* = temperature below which reaction is first order. Experimental: same as for Fig. 20.

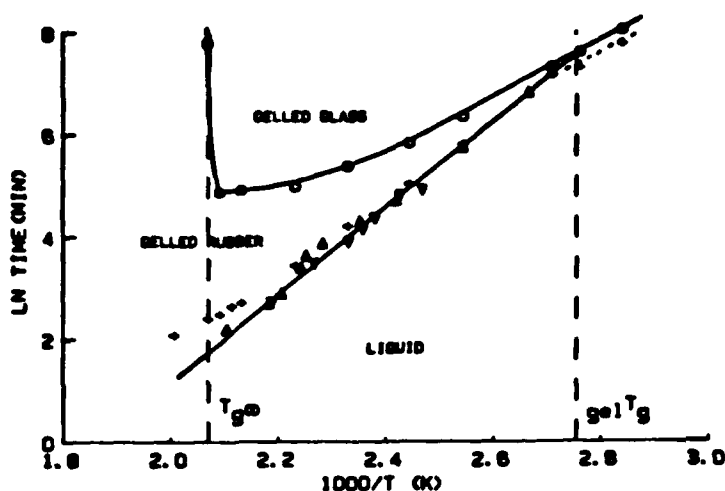


Fig. 22. TTT cure diagram in terms of log time vs. $1/T$ (K) for Epon 828/DDS. TBA: (O) vitrification; (+) liquid-to-rubber transformation. Gel fraction: (Δ) helium; (∇) air. Note that in this system the pregel event is not observed. Epon 828 is a diglycidyl ether of bisphenol A (Shell Chemical Co.). DDS is diamino diphenyl sulfone (Aldrich).

the temperature range from which the TBA and RDS data were taken to calculate the activation energy, it would explain the low values obtained by these techniques (Table VIII). Gel fraction data were obtained only below 90°C , and all but two IR experiments were performed at temperatures below 90°C . If the IR data below 90°C only are analyzed, the revised activation energy from the IR data is 13.3 kcal/mol.] By using a weighted average of first- and second-order kinetics beginning at $T^* = 1.3$, and first-order kinetics below $T^* = 1.3$, the model gives an excellent fit to the data over the entire range (Fig. 21).

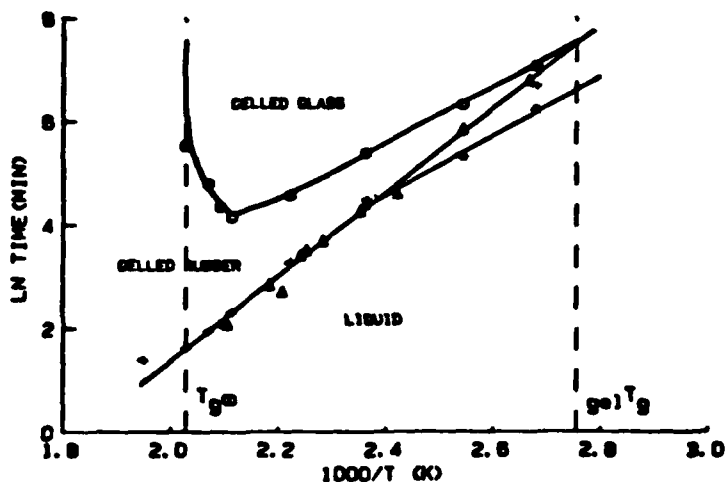


Fig. 23. TTT cure diagram in terms of log time vs. $1/T$ (K) for Epon 825/DDS. TBA: (O) vitrification; (+) liquid-to-rubber; (•) pregel. Gel fraction: (∇) air. Epon 825 is a diglycidyl ether of bisphenol A (Shell Chemical Co.).

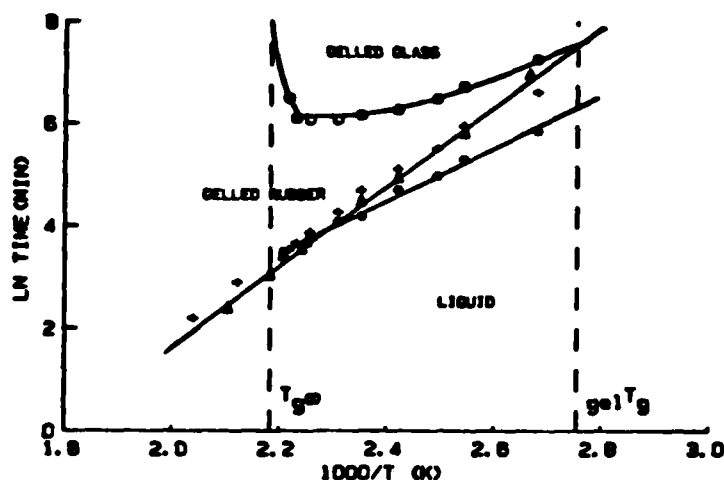


Fig. 24. TTT cure diagram in terms of log time vs. $1/T$ (K) for Epon 834/DDS. TBA: (O) vitrification; (+) liquid-to-rubber; (•) pregel. Gel fraction: (∇) air. Epon 834 is a diglycidyl ether of bisphenol A (Shell Chemical Co.).

CONCLUSIONS

The cure of a thermosetting resin can be described by a TTT cure diagram showing the times to gelation and to vitrification as a function of isothermal cure temperature. For a given system it is defined by the physical parameters of the resin, (T_{g0} , $gel T_g$, and $T_{g\infty}$), the reaction kinetics, and the relationships between the extent of conversion and gelation, and the extent of conversion and the glass transition temperature. The TTT cure diagram for Epon 828/PACM-20, constructed from TBA, RDS, gel fraction, and FT-IR experiments, is qualitatively comparable with a theoretically derived TTT diagram. The comparison suggests that there may be a change in reaction mechanism from first order to a mixture of first- and second-order kinetics at 85°C, and demonstrates the utility of this type of analysis for thermosetting systems.

APPENDIX: MEASUREMENT OF GELATION TIMES

In order to construct a TTT cure diagram, measurements of the times to vitrification and to gelation are required. The TBA technique gives an unambiguous assignment of vitrification in terms of the time (and a frequency) at which a peak occurs in the mechanical damping (logarithmic decrement) in conjunction with an increase in modulus. An attempt has been made in this report to identify the macroscopic liquid-to-rubber transformation with the onset of molecular gelation. The former was assigned to the mechanical loss peak occurring immediately prior to that for vitrification in the TBA experiment: the latter was assigned by the onset of insolubilization in gel fraction experiments. The correlation between these macroscopic and molecular observations was not as good for the Epon 828/PACM-20 system (Fig. 17) as it is for other systems. Three examples for which the correlation is better are shown in Figures 22-24.

This research was partially supported by the Army Research Office.

References

1. J. K. Gillham, "Torsional Braid Analysis (TBA) of Polymers," in *Developments in Polymer Characterisation*—3, J. V. Dawkins, Ed., Applied Science, London, 1982, Chap. 5.
2. P. J. Flory, *Principles of Polymer Chemistry*, Cornell University Press, Ithaca, N.Y., 1953.
3. S. Lunak, J. Vladyka, and K. Dusek, *Polymer*, **19**, 931 (1978).
4. J. B. Enns and J. K. Gillham, in *Polymer Characterization: Spectroscopic, Chromatographic, and Physical Instrumental Methods*, C.D. Craves, Ed., *Am. Chem. Soc., Adv. Chem. Ser.*, **203**, (1983), Chap. 2.
5. H. N. Nat and J. K. Gillham, *Am. Chem. Soc., Div. Org. Coatings Plast. Chem., Prepr.*, **48**, 566 (1983).
6. J. B. Enns, Ph.D. thesis, Princeton University, 1982.
7. J. B. Enns and J. K. Gillham, *Am. Chem. Soc., Div. Org. Coatings Plast. Chem., Prepr.*, **47**, 575 (1982).
8. H. E. Adabbo and R. J. J. Williams, *J. Appl. Polym. Sci.*, **27**, 1327 (1982).
9. A. T. Di Benedetto, in L. E. Nielsen, *J. Macromol. Sci., Rev. Macromol. Chem.*, **C3**, 69 (1969).
10. K. Horie, H. Hiura, M. Sawada, I. Mita, and H. Kambe, *J. Polym. Sci., A-1*, **8**, 1357 (1970).
11. W. Fisch, W. Hofmann, and R. Schmid, *J. Appl. Polym. Sci.*, **13**, 295 (1969).
12. H. P. Gray, "Thermal Analysis Application Study 2," Perkin-Elmer Corp., 1972.
13. J. M. Barton, *Polymer*, **21**, 603 (1980).
14. M. R. Kamal, *Polym. Eng. Sci.*, **14**, 231 (1974).
15. M. Gordon and W. Simpson, *Polymer*, **2**, 383 (1961).
16. R. B. Prime, "Thermosets," in *Thermal Characterization of Polymer Materials*, E. A. Turi, Ed., Academic, New York, 1982, Chap. 5.
17. T. G. Fox, S. Gratch, and S. Loshaek, in *Rheology*, F. R. Eirich, Ed., Academic, New York, 1956, Vol. 1, p. 440.
18. G. C. Berry and T. G. Fox, *Adv. Polym. Sci.*, **5**, 261 (1968).
19. D. W. Sundstrom and S. J. Burkert, *Polym. Eng. Sci.*, **21**, 1108 (1981).
20. M. B. Roller, *Polym. Eng. Sci.*, **15**, 406 (1975).
21. J. D. Ferry, *Viscoelastic Properties of Polymers*, 3rd ed., Wiley, New York, 1980.
22. C. W. Macosko and D. R. Miller, *Macromolecules*, **9**, 199 (1976).
23. D. R. Miller and C. W. Macosko, *Macromolecules*, **11**, 656 (1978).
24. J. B. Enns and J. K. Gillham, in *Computer Applications in Applied Polymer Science*, T. Provder, Ed., ACS Symposium Series No. 197, Am. Chem. Soc., Washington, D.C., 1982, Chap. 20.
25. G. A. Pogany, *Polymer*, **11**, 66 (1970).
26. M. Ochi, M. Okazaki, and M. Shimbo, *J. Polym. Sci., Polym. Phys. Ed.*, **20**, 689 (1982).
27. C. C. Kuo, C. Y.-C. Lee, and I. J. Goldfarb, *Am. Chem. Soc., Div. Org. Coatings Plast. Chem., Prepr.*, **47**, 595 (1982).
28. I. J. Goldfarb, C. Y.-C. Lee, and C. C. Kuo, *Am. Chem. Soc., Div. Org. Coatings Plast. Chem. Prepr.*, **47**, 600 (1982).
29. J. P. Aherne, J. B. Enns, M. J. Doyle, and J. K. Gillham, *Am. Chem. Soc., Div. Org. Coatings Plast. Chem. Prepr.*, **46**, 574 (1982).
30. J. B. Enns and J. K. Gillham, *J. Appl. Polym. Sci.*, **29**, (1983), to appear.
31. S. C. Lin, B. J. Bulkin, and E. M. Pearce, *J. Polym. Sci., Polym. Chem. Ed.*, **17**, 3121 (1979).
32. P. G. Babayevsky and J. K. Gillham, *J. Appl. Polym. Sci.*, **17**, 2067 (1973).
33. G. Odian, *Principles of Polymerization*, Wiley, New York, 1981.
34. J. B. Enns, unpublished data.
35. T. R. McCalla, *Introduction to Numerical Methods and FORTRAN Programming*, Wiley, New York, 1967.

Received March 16, 1982

Accepted in revised form March 21, 1983

4 .
3 .
2 .
1 .

SCIENTIFIC PERSONNEL

J. K. Gillham, Professor, Principal Investigator.

J. B. Enns, Graduate Student, Ph.D., Princeton University, June 1982.

M. Aronhime, Graduate Student.

L. Chan, Graduate Student.

X. Peng, Post-doctoral.

END

FILMED

11-83

DTIC